Spectroscopy of low-coordinated surface sites: Theoretical study of MgO

Alexander L. Shluger

Department of Physics and Astronomy, University College London, Gower Street, London WC1E 6BT, United Kingdom

Peter V. Sushko

Department of Physics and Astronomy, University College London, Gower Street, London WC1E 6BT, United Kingdom
and The Royal Institution of Great Britain, 21 Albemarle Street, London W1X 4BS, United Kingdom

Lev N. Kantorovich

Department of Physics and Astronomy, University College London, Gower Street, London WC1E 6BT, United Kingdom

(Received 25 August 1998)

We demonstrate a dramatic dependence on the oxygen coordination of the calculated optical absorption and luminescence energies of low-coordinated sites at the surfaces and in nanoclusters of MgO. The calculations for $(MgO)_{256}$ cubic nanoclusters were performed using an embedded molecular cluster model and both semi-empirical and *ab initio* Hartree-Fock methods. The optical-absorption energies were calculated using the configuration interaction technique for single (CIS) and double electronic excitations. The luminescence energies were calculated using the CIS method. The low-coordinated sites included corners, kinks, step and cluster edges, and corner vacancy defects. We have also studied the zigzag steps and monatomic steps at infinite surfaces using a periodic density-functional theory method and a plane-wave basis set. For both the nanoclusters and infinite surfaces, the results show a consistent significant reduction of the exciton excitation energies and of the luminescence energies of relaxed excitons as the oxygen coordination decreases. We also demonstrate the possibility of exciton transfer from the sites with higher coordination to those with lower coordination and finally to the localization centers. Selective optical excitation of low-coordinated surface sites could be used to study molecular adsorption at surface sites, photocatalytic surface processes and desorption induced by electronic transitions. [S0163-1829(99)07203-3]

I. INTRODUCTION

Atomic coordination has long been recognized as one of the most important factors in determining the chemical and spectroscopic properties of surface sites. Although the effect is general, its mechanism depends on the character of chemical bonding. In this paper, we focus on the spectroscopic properties of low-coordinated sites in ionic oxides, such as MgO. The reduced ion coordination in these crystals leads to significant changes in the crystalline potential,[1] which have been correlated with the chemical (see, for example, recent discussion[2]) and spectroscopic[1,3] properties of the low-coordinated surface sites. Experimentally, several spectroscopic features have been attributed to the presence of these sites. In particular, the high-resolution electron energy loss spectra of MgO have demonstrated that the exciton absorption peak shifts from 7.7 eV in the bulk[4] to 6.15 eV at the (001) surface plane.[5] The ultraviolet diffuse reflectance spectra of microcrystalline MgO have demonstrated the additional bands at 5.7 and 4.6 eV, which have been attributed to the low-coordinated sites, such as steps, kinks, and corners.[3,6] Coluccia and co-workers[7–10] have studied the photoluminescence of powdered MgO excited in these bands and have observed broad luminescence spectra. Both the excitation and emission spectra demonstrate a strong dependence on the powder preparation and treatment with different gases.[8,9] They were attributed to the excitation and luminescence of excitons at different low-coordinated sites at powder surfaces. Very similar features have been observed in the

excitation and emission spectra of the other cubic oxides CaO, SrO, and BaO.[6–10] An alternative model of photoluminescence from powdered MgO and CaO suggested by Duley[11] involves the F^+ surface centers in addition to the low-coordinated oxygen sites.

The proposed interpretation of these experimental data implies a dramatic dependence of the spectroscopic properties of oxide surfaces on the ion coordination. In particular, the exciton excitation energy is thought to be reduced from 7.7 eV in the bulk to about 4.6 eV at the three-coordinated sites. The luminescence lifetimes estimated in Ref. 7 are about several microseconds or longer. These relatively long lifetimes could be due to transitions from a localized triplet excited state as, for example, the triplet luminescence of the self-trapped excitons in alkali halides.[12] Coluccia and co-workers[7,8] proposed a model of the exciton at the surface of cubic oxides according to which the optical excitation is accompanied by an electron transfer within a pair of O and Mg ions. In the completely ionic model this corresponds to the process: $Mg^{2+} - O^{2-} + h\nu \Rightarrow Mg^+ - O^-$. If this model is correct, the long luminescence lifetime could also be due to the electron tunneling within a pair of the low-coordinated O^- and Mg^+ ions. Thus, the nature of the luminescence state is still unclear.

Further experimental verification of these models is presently very difficult. Their theoretical understanding requires detailed analysis of the nature of the excited states. Using the values of the Madelung potential at different surface sites and other considerations Garrone, Zecchina, and Stone[3] have

attributed the experimentally observed features in the ultraviolet diffuse reflectance spectra of MgO microcrystals at 6.6, 5.75, and 4.62 eV to the five-, four-, and three-coordinated surface sites, respectively. The calculated[13] polarizabilities of oxygen ions at low-coordinated surface sites of MgO increase as the coordination decreases, which indicates the decrease of optical excitation energies. Pandey, Zuo, and Kunz[14] and Bagus, Illas, and Sousa[15] studied the lowest excited states in the bulk of MgO. The embedded cluster calculations by Pandey, Zuo, and Kunz[14] suggest complete exciton localization on the oxygen ion. The more conventional cluster calculations by Bagus, Illas, and Sousa[15] demonstrated an opposite behavior of the excited electron: it is completely delocalized over the entire cluster. However, quantum mechanical calculations for excited states at surfaces with different low-coordinated sites, except for the plane (001) MgO surface,[16] are missing.

Further studies of surface spectroscopic properties are important for the understanding of different modes of exciton localization in the bulk and at surfaces of oxides, and of the energy transfer from excitation sites to luminescent centers. The latter is relevant to the mechanisms of desorption induced by electronic transitions (DIET) and to other photoinduced surface reactions. The demonstrated sensitivity of the spectroscopic surface properties to adsorption of gases[8,9] could be used to study site selectively molecular adsorption and chemical reactions at surfaces. Therefore, the aims of this study are: (i) to verify whether the reflectance spectra and photoluminescence data obtained on microcrystalline and powdered samples of MgO could be understood on the basis of excitation and luminescence at different low-coordinated surface sites; and (ii) to study the nature and degree of localization of different excited states at the MgO surfaces.

The low-coordinated sites which are possibly contributing to the spectra are not well defined. Therefore to have a convincing set of data we used several surface models. According to the electron micrographs[8,17] of the powders used in the photoluminescence experiments, one can view them as an assembly of microclusters of different shapes and sizes. Most of them are cubic, but they become more rough at edges and corners after additional treatments.[8] Powders of clusters as small as several nanometers across can be now produced using molecular beam sources.[18,19] Therefore, one can reasonably consider the problem of optical properties of powders as that of interacting nanoclusters. Since very little is known about the optical properties of nanoclusters of oxides, this consideration adds another dimension to this study. In this paper, we considered cubic clusters more than 1 nm across with ideal shape and also clusters with steps and kinks on their grains. In order to have convenient notations through the paper we will denote these finite clusters as ''nanoclusters.'' To study similar effects at low-coordinated sites of infinite surfaces, we used a periodic surface model of steps and kinks.

Calculation of excited states in crystals is still not an easy task. One of the main problems concerns the relation between the degree of localization of the excited state and the size of the system treated quantum mechanically. For such complex low-symmetry systems as considered in this paper one is always looking for a compromise between the accuracy of the technique and the size of the system studied. Our approach was to first make a pilot study for the simplest archetypal sites in cubic nanoclusters using an embedded cluster model and an *ab initio* Hartree-Fock method together with the configuration interaction techniques including single and double excitations for calculation of the excited states. The idea was to see whether we will obtain the right tendency in excitation energies as a function of oxygen coordination using the simplest models and the most accurate techniques available to us, and to use these results as a benchmark for further calculations. Then we applied a semiempirical Hartree-Fock method in order to study more complex surface sites that require larger number of quantum ions, and to calculate the relaxed excited states and the luminescence energies. However, both these series of calculations used cluster models and localized basis sets and could not give definite answers with regard to the nature and degree of localization of the excited states. To address these issues further we used a periodic model and a computational technique based on a density-functional theory (DFT) and a plane-wave basis set. As we will see below, each of these techniques has its drawbacks but in combination they provide a reliable model for the spectroscopy of the low-coordinated surface sites. The methods of calculations are discussed in Sec. II, the results are presented in Sec. III, and the conclusions are discussed in Sec. IV.

II. METHODS OF CALCULATION

A. Cluster methods

The nanoclusters considered in this study consist of several hundred ions, therefore, the most effective way to calculate the geometric and electronic structures of different surface sites is to embed a quantum cluster at a place of interest. In order to do that we divide our system into individual ions, which is a good approximation for highly ionic materials such as MgO. This allows us to use the pair interionic potentials to calculate the nanocluster geometry with good accuracy. This is done using the atomistic simulation technique implemented in the General Utility Lattice Program (GULP) code.[20] More importantly, in this approximation we can substitute a number of ions in the nanocluster by a quantum cluster and combine a quantum-mechanical treatment of the quantum cluster with the classical treatment of the rest of the nanocluster to describe the whole system. For *ab initio* Hartree-Fock calculations we employed the GAUSSIAN94 code[21] where this is achieved by adding the matrix elements from point charges to the Fock matrix of the quantum cluster. A more sophisticated treatment that allows one to account for polarization of the nanocluster due to electronic excitation or other defect localized in the quantum cluster, is realized in the semiempirical CLUSTER95 code.[22,23] The detailed discussion of the technique in conjunction with the calculations of point defects in the bulk of ionic crystals was given in Ref. 22. Therefore, we will focus mainly on its peculiarities with respect to the nanocluster calculations and on technical details that are necessary for understanding of the results of this paper.

Ab initio cluster method

We used the GAUSSIAN94 code[21] to calculate the optical excitation energies, the singlet-triplet splitting, and to check the importance of electron correlation in the optical excitation energies for basic low-coordinated sites in the nanoclusters. A quantum cluster was embedded in a nanocluster of nonpolarizable ions. The initial geometry of the whole nanocluster was calculated by the GULP code using pair potentials and then fixed. The Buckingham-type pair potentials used in this study are described in Refs. 24 and 25. In order to prevent an artificial delocalization of the defuse electronic states, the nearest and the next-nearest cations surrounding the quantum clusters carried the pseudopotentials of Wadt and Hay.[26] The interaction with all other point ions in the nanocluster was calculated using the standard procedure[27] incorporated in GAUSSIAN94. Both diagonal and nondiagonal matrix elements of the Coublomb potential of these ions are included in the Fock matrix.

Technical details of the *ab initio* calculations are as follows. All electrons of the quantum cluster were included in the calculations. For comparison, we used two different basis sets: (i) the standard $6311+G$ basis set for both Mg and O ions (set A); and (ii) the basis sets that were developed for the O and Mg ions by Bagus and co-workers,[28,29] and latter was employed in the calculations of the excited state of the MgO clusters[15] (set B). The second basis set is much more contracted than the first one, which is advantageous in terms of computational time. It was optimized for the free O^- ion that might be beneficial for the calculations of the excited states. Natural population analysis[30] was used throughout all GAUSSIAN94 calculations.

The excitation energies were calculated using two techniques: (i) the configuration interaction technique for single electron excitations[31] (CIS), and (ii) as a difference between the total energies of the singlet and the triplet states of the system calculated using the configuration interaction technique that accounts for single- and double-excited electron configurations[32] (CISD). The latter method allows us to take into account part of the electron correlation in both ground and excited states. The CASSCF (complete active space self-consistent field) method that can provide a better treatment of both ground and excited states was not used since it appeared to be computationally too demanding. Therefore, only the singlet-triplet transitions were calculated using the CISD method.

Semiempirical embedded cluster method

Calculation of the embedding potential. In the CLUSTER95 code, the electronic structure of the quantum cluster is calculated using the unrestricted Hartree-Fock (UHF) method within the approximation of intermediate neglect of differential overlap[33,34] (INDO). In this approximation some of the elements of the Fock matrix are calculated using semiempirical parameters. The set of parameters used in this study was optimized in order to reproduce the characteristics of the MgO perfect crystal as well as an extensive set of other oxides and small molecules, as described in Ref. 34.

The nanoclusters considered in this study have different shapes, sizes, and defects. Some of them are simply cubic clusters, others have steps, kinks, and vacancies included (see, for example, Fig. 1). The main differences of the embedded cluster model employed in the CLUSTER95 code with respect to a commonly used method of embedding into the potential of an array of point charges discussed above are the following: (i) The interactions between the ions outside the quantum-mechanical cluster are treated using the interionic potentials, and their polarizability is accounted for using the shell model.[35] (Note that cores and shells in this model are just point charges with the total charge equal to the ionic charge.) (ii) The system total energy is minimized with respect to the positions of the quantum ions and those of the cores and shells comprising the classical ions. This approach allows us to study the geometric structures of the nanoclusters as a function of their size, shape, and presence of the structural defects, and to calculate the additional polarization of the nanocluster by the exciton. (iii) The electronic and geometric structures of the quantum cluster are calculated self-consistently with the embedding potential due to the remaining ions in the nanocluster using the procedure described in Ref. 22.

The embedding potential includes the short-range contribution and the long-range (electrostatic) contributions due to the (polarized) ions. The ions outside the quantum cluster are polarized by the additional electric field due to the change in the charge-density distribution $\Delta\rho$ inside the quantum cluster produced, in our case, by the electron excitation. $\Delta\rho$ is calculated with respect to the initial charge distribution within the entire nanocluster before the electron excitation using the Löwdin population analysis to calculate the effective charges. These calculations demonstrated that the effective charges on the ions in the interior of the nanoclusters far from the surface are close to those in the bulk of a crystalline MgO and decrease systematically as the coordination decreases. Similar behavior of the ionic charges has been observed in Ref. 2. This provides a reference charge distribution for each particular nanocluster.

Calculations for each new nanocluster start from the total geometry optimization using pair potentials and the GULP code.[20] The same program is used to optimize the positions of cores and shells outside the quantum cluster in response to the changes in the charge distribution inside the quantum cluster. Compatibility of the quantum-mechanical and classical descriptions is achieved at the stage of their parametrization: both techniques give the same lattice constants for the bulk crystal and the same geometric parameters for the finite clusters. Comparison of the bond lengths and angles for several clusters calculated using the GULP, the INDO method, and the GAUSSIAN94 code with different basis sets has demonstrated agreement within 1–2%.

The total energy of the whole system including the quantum cluster embedded in the nanocluster is minimized with respect to the linear combination of atomic orbitals coefficients, positions of the nuclei inside the quantum cluster and of the cores and shells of the rest of the nanocluster. The calculations of the polarization and of the electronic structure and the geometry of the quantum cluster embedded in the electrostatic potential of the polarized nanocluster are carried out iteratively until the total energy of the whole system changes between iterations by less than 0.001 eV.

On the programming level, the computations are organized using an interface between the quantum-mechanical and the classical (GULP) codes. This proved to be a very

flexible procedure that allows us to introduce only slight modifications to the Hartree-Fock and the GULP codes due to their combined use.

Calculation of the excitation and luminescence energies. Although the configuration interaction method including single-electron excitations (CIS) can provide reasonable accuracy of excitation energies, this is not the most straightforward technique for calculating relaxed excited states and luminescence energies. In fact the simplest way to find the lowest relaxed excited state in wide gap insulators is the self-consistent calculation of the triplet state. However, the single determinant of the UHF method is not always a good approximation for the wave function of the excited state. Another drawback associated with this approach is that it involves comparison of the results of two different techniques: the restricted and unrestricted Hartree-Fock methods used for calculations for the ground and excited state, respectively. Therefore, we used the CIS method to calculate both the excitation and luminescence energies.

The CLUSTER95 code allows us to calculate only singlet-singlet transitions using the CIS method. These calculations, though, cannot be performed self-consistently with the polarization of the rest of the nanocluster. We believe that neglect of electronic polarization in the excited state does not affect significantly the calculated *excitation* energies corresponding to the vertical transitions. However, ionic displacements and their electronic polarization can be much more important in the calculations of the relaxed excited states, which are needed to obtain the *luminescence* energies. Therefore, to calculate the singlet-singlet luminescence energies we employed the following approximate method.

The idea of this method relies on the observation that the electron densities of the quantum cluster after the singlet and triplet excitations obtained using CIS in our *ab initio* calculations are very similar. This implies similar polarization of the rest of the nanocluster. We use this feature in the following way.

(i) First, we calculate the triplet-excited state of the quantum cluster using the UHF method self-consistently including the polarization of the nanocluster. The positions of ions in the quantum cluster $\mathbf{R}$ are optimized to achieve the minimum of the total energy. As was mentioned above, since the polarization effects are expected to be similar, we can fix the calculated positions of the cores of the rest of the nanocluster $\mathbf{R}_c$ throughout the next series of the calculations. (ii) Using the positions $\mathbf{R}$ of the atoms in the quantum cluster, the ground singlet state is calculated keeping the cores $\mathbf{R}_c$ fixed. The shells were allowed to relax. (iii) Using the CIS method, we calculate the spectrum of the one-electron excitations from this ground state with fixed $\mathbf{R}$, $\mathbf{R}_c$, and shells. To calculate the luminescence associated with a particular singlet-excited state, one has to identify this state in the spectrum. This is done by picking up the state e with the biggest transition-matrix element and with the orientation of the transition-dipole moment corresponding to the charge transfer in the original triplet state. (iv) The positions of atoms in the quantum cluster are varied and the adiabatic potential energy surfaces $\mathbf{E}_{gs}(\mathbf{R})$ and $\mathbf{E}_{exc}(\mathbf{R}) = \mathbf{E}_{gs}(\mathbf{R}) + \Delta\mathbf{E}_{exc}^e(\mathbf{R})$ for the singlet-ground and excited states, respectively, are calculated using the excitation energies $\Delta\mathbf{E}_{exc}^e(\mathbf{R})$. When the minimum of $\mathbf{E}_{exc}(\mathbf{R})$ is found, it is associated with the initial

state for the luminescence, and the luminescence energy is estimated as $\mathbf{E}_{exc}(\mathbf{R}) - \mathbf{E}_{gs}(\mathbf{R})$.

Throughout all these calculations we keep the positions of the cores $\mathbf{R}_c$ fixed as obtained in the initial triplet state. To adjust the polarization, we recalculate the triplet state for the optimized configuration of ions in the quantum cluster $\mathbf{R}$ and repeat the whole cycle (i)–(iv) again until both the luminescence energy and the atomic positions are consistent.

This method allows us to obtain simultaneously, and within the same approximation, the adiabatic potentials for the singlet-ground and excited states. In the excited state, the full polarization of the nanocluster is accounted for, and in the ground state the electronic part is adjusted to the new electron configuration. Therefore, the energy difference with the ground state calculated at the minimum of the excited state energy surface corresponds to the Franck-Condon luminescence energy.

B. Density-functional method

In the cluster methods discussed above, the degree of localization of the excited state and its symmetry can be imposed by a small size and a particular symmetry of the quantum cluster, and by the localized basis sets employed in the calculations. To relax both of these conditions, one can make calculations using periodic boundary conditions and the plane-wave basis sets. There remain restrictions imposed by the size and a symmetry of a particular unit cell and by the calculation technique. Nevertheless, comparison of the results of the periodic and cluster calculations using different basis sets and methods can provide deeper insight into the problem.

In this paper, the periodic DFT calculations were made using the Car-Parrinello technique,[36] in which the total energy of the system is minimized with respect to the plane-wave coefficients of the occupied orbitals. Two realizations of this technique were employed, which are implemented in two different computer codes. In the first of them, the CETEP code,[37] the normconserving pseudopotentials in the Kleinman-Bylander form[38] are implemented. The pseudopotentials for Mg and O ions and the plane-wave cutoff of 850 eV used in this study are identical to those used in the recent studies of the oxygen adsorption at the MgO surface.[39,40] The conjugate gradient technique[41] was used to perform both the electronic and ionic relaxations. The details of the computational strategy underlying the CETEP code has been published elsewhere.[37] To compare the results, we performed the same calculations using also the VASP code[42,43] where ''soft'' Vanderbilt pseudopotentials[44,45] are implemented. The electronic relaxation in our VASP calculations is performed using iterative methods, while the conjugate gradient method is employed to perform the ionic relaxation. However, the main difference between the both codes is in the pseudopotentials: in the VASP code the normconservation condition for the pseudopotentials is relaxed thereby reducing the cutoff down to about 400 eV. This speeds up the calculation by a factor of 3–5 in spite of a more complicated computational scheme.

Calculations by both methods are based on the generalized gradient approximation functional of Perdew and Wang[46,47] known as GGA-II and are designed for general spin-polarized systems. They were performed for a periodic slab geometry. In this model, a unit cell is repeated in two

dimensions creating an infinite slab simulating the (001) surface. The slabs are repeated in the z direction (normal to the surface) forming a stack of layers separated by a vacuum layer. Our choices of the slab thickness and vacuum width are discussed below. The question of **k**-point sampling for calculations of the (001) MgO surface has been discussed in recent publication.[39] Two **k**-points in the surface Brillouin zone were used in most of our surface calculations, and four **k** points for symmetric unit cells. All the calculations were performed at the Edinburgh Parallel Computer Center on Cray T3D/T3E parallel supercomputers.

It is well known that the DFT method is designed only for calculating the lowest states of any multiplicity,[48] therefore, we can only study the singlet-triplet transitions. At this point, we note that the singlet state of the MgO molecule calculated using the CETEP code has the equilibrium distance 1.743 Å and is 0.36 eV lower than the triplet state, in good agreement with experiment.[49] The excitation (singlet-triplet) and luminescence (triplet-singlet) energies were calculated in the following way. First, we find the ground singlet state of the system in question with all atoms in the slab allowed to relax to mechanical equilibrium. Then, keeping all the atoms in the positions obtained for the ground state, the triplet state was calculated. The energy difference between the fully relaxed electronic configuration in the triplet state and the ground state corresponds to the Franck-Condon singlet-triplet excitation energy. To calculate the luminescence energy, we first relax the slab atoms in the triplet state; only atoms of the bottom layer are kept fixed. This gives us the fully relaxed triplet excited state of the system. Finally, for this atomic configuration a singlet state is calculated. The corresponding energy difference is associated with the luminescence energy of the vertical triplet-singlet transition.

III. RESULTS OF CALCULATIONS

The low-coordinated surface sites considered in this study are shown in Figs. 1 and 4. Based on the significant changes in the excitation spectra of photoluminescence due to the additional treatment of MgO powders by water and some gases, Coluccia and co-workers speculated that cation and anion vacancies at the corner sites could be important.[7,8] Therefore, they were also included in the calculations. Although it is clear that the variety of possible excitation sites is more diverse, the types shown in Figs. 1 and 4 seem to be already fairly representative. Different sites have different cross sections for photon absorption and contribute to different parts of the spectra. In particular, the number of cube corners is smaller than those of steps and kinks. However, in this paper we are mainly concerned with the site dependence of the excitation and luminescence energies.

An important issue is how to compare the results obtained using several different techniques. The geometric parameters of the systems calculated using the atomistic simulation technique, the two embedded cluster methods and the DFT techniques are very similar. We have compared the results for the Mg_4O_4 clusters, and for step relaxation at the MgO surface[39,50] and the agreement of the bondlengths and angles is within 2%. Comparison of the absolute values of excitation and luminescence energies is less straightforward due to the differences in the techniques, which are difficult to con-
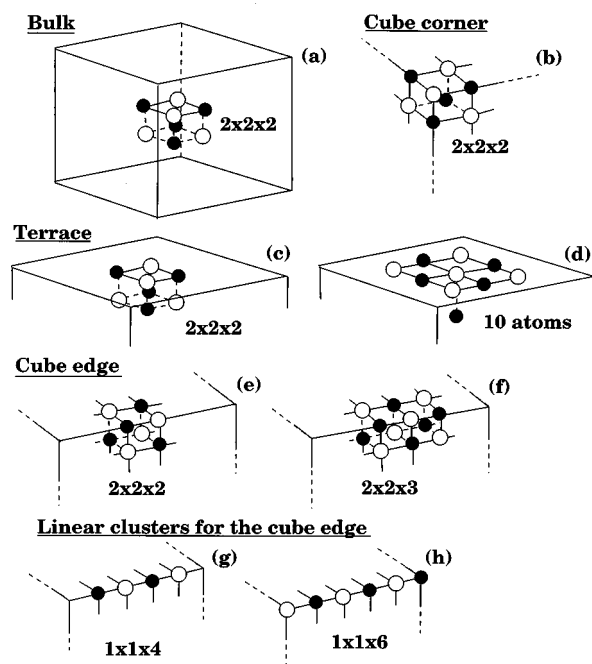

FIG. 1. Schematic of quantum clusters embedded into a 6×6×6 256-ion nanocluster used in *ab initio* Hartree-Fock and beyond Hartree-Fock calculations of excitation energies of low-coordinated sites. Open circles are oxygen ions and black circles are magnesium ions.

trol, such as the electron correlation accounted for by INDO parameters and by a particular DFT functional. The most accurate values for the excitation energies are expected by the CISD method. As we will see below, the energies given by other methods do not differ dramatically from the CISD results, however the most meaningful comparison is between the relative energies for different surface sites.

Finally, prior to discussing the results of calculations for the excited states, let us summarize the geometric structure of the nanoclusters and of the steps and kinks at the MgO surface. There is no need for longer discussion since relevant data have already been published in several papers, including the calculations performed with the same methods as employed in this study.[39,50,51] The general trend in relaxation of steps, edges, corners, and kinks of ionic crystals is well known: it tends to smooth out the discontinuity. The inward displacements of border ions are quite substantial and amount to about 6–8 % of the bulk lattice constant in most of the calculations. These displacements calculated for the step and the step corner and the (001) MgO surface using the DFT method are given in Ref. 39. The additional feature characteristic for nanoclusters is the distribution of interionic distances as a function of the ions position with respect to the cluster borders. The cluster shape is rounded with respect to the ideal rectangular form. The interionic distances are smallest at the corners and largest in the ''bulk'' of a cluster. Very accurate numerical values are difficult to obtain because the only source of data for large clusters are the calculations using interatomic potentials. These calculations do not take into account the changes in the electronic structure of ions as a function of their coordination. However, a qualitative trend can be seen from the results of our GULP calculations using the pair potentials given in Ref. 24. For the cubic clusters of 64, 216, and 512 ions, the interionic sepa-

TABLE I. The excitation energies for different sites in the cubic $(MgO)_{108}$ nanocluster calculated using the CIS and CISD techniques, and two different basis sets (eV).

Lowest oxygen coordination	Position	Number of atoms (Fig. 1)	Basis set	CIS[a]			CISD	
				$S \to T$	$S \to S$	Δ[b]	$S \to T$	$(S \to S)$[c]
6	Bulk	8 (a)	A	8.9	8.9	0.0	7.5	7.5
			B	11.3	12.3	1.0	10.7	
5	Terrace	8 (c)	A	7.1	7.8	0.7	6.4	7.1
			B	7.9	8.7	0.8	7.1	
		10 (d)	A	7.2	7.9	0.7		
4	Edge	8 (e)	A	6.1	6.8	0.7	5.0	5.7
			B	7.3	7.9	0.6		
		12 (f)	A	6.1	6.9	0.8		
		6 (h)	A	5.6	6.1	0.5		
		4 (g)	A	5.6	6.5	0.9		
3	Corner	8 (b)	A	5.3	5.8	0.5	4.0	4.5
			B	5.5	6.1	0.6	4.3	

[a]The CIS energies are given for the excitations with the largest transition-matrix element.

[b]The singlet-triplet splitting energy.

[c]These energies are calculated by adding the CIS singlet-triplet splitting energy Δ to the CISD excitation energy into the triplet state.

rations at the anion corner are about 1.91 Å in all cases. The distance between nearest ions inside the cluster increases from 2.05 Å for the 64-ion cluster to 2.07 Å for that of 512 ions (the bulk value is 2.105 Å). Similar trend has been obtained in recent density-functional calculations for the cubic MgO clusters containing up to 64 ions.[52]

A. *Ab initio* calculations for nanoclusters

Quantum clusters of different sizes were embedded at the oxygen corner and at the edge, grain, and in the bulk of a (MgO) 108 cubic nanocluster (see Fig. 1). The geometry of this $(6 \times 6 \times 6)$ nanocluster was optimized using the pair potentials and the GULP code and was kept fixed in all the calculations of this series.

The calculated energies for the transitions with the largest oscillator strength are summarized in Table I. One can immediately see a trend: independent of the basis, the excitation energies into the singlet and triplet states decrease gradually as the coordination of the oxygen ion decreases. To compare different basis sets and techniques, we can use the experimental values of the exciton excitation energies in the bulk and at the (001) surface plane. The reflectance spectra of MgO single crystals[4] measured at 77 K demonstrate a singlet-triplet splitting with the triplet pick at 7.69 eV and the singlet pick at 7.76 eV. The high-resolution electron-energy loss (HREEL) spectra of the (001) surface[5] demonstrate an exciton peak at about 6.15 eV. At high coordinations, the excitation energies calculated using the basis set by Bagus and co-workers (B) are much larger than both the experimental values and the results obtained with the basis set A. The differences between theoretical results are much smaller for the edge and corner where the oxygen configuration is closer to the O^- ion configuration used[28] for the optimization of the basis B.

The excitations into the triplet state have lower energies than those into the singlet state. The singlet-triplet splittings

for the different low-coordinated sites calculated using CIS are given in Table I. One can see that they depend significantly on the basis set, the oxygen coordination, and the cluster size. The excitation energies calculated using CISD have much lower energies than those obtained with CIS, revealing the importance of the electron correlation.

The effect of the size and shape of the quantum cluster on the calculated excitation energies can be seen in Table I where we compare the results for different clusters. In four cases the calculations were made for a cubic cluster Mg_4O_4 embedded in different positions inside the nanocluster [see Figs. 1(a)–1(c) and 1(e)]. The disadvantage of this quantum cluster is that the ions are treated differently at different positions in the nanocluster. For instance, the corner oxygen ion is fully surrounded by the cations with a basis set [Fig. 1(b)]. However, at the edge [Fig. 1(e)] the fourth cation nearest to the edge oxygen ion is a bare pseudopotential and does not carry a basis. To check whether this may introduce any significant difference in the calculated energies we have considered larger clusters where one of the oxygen ions was fully coordinated by quantum ions (see Table I). For the edge, we expanded the cube by another four ions [the 12-ion cluster in Fig. 1(f)] and also considered two linear clusters comprising four and six ions located along the edge (Figs. 1(g), 1(h)). For the surface, we took a completely different cluster which is shown in Fig. 1(d). It has nine ions in the surface plane with the oxygen ion in the center, and an additional Mg ion in the second plane just below the central oxygen. The results of the CIS calculations presented in Table I demonstrate that the excitation energies change within 0.5 eV, with the largest difference between the cubic and linear clusters at the edge.

To demonstrate the character of the electron localization, in Fig. 2 we present sections of the spin-density maps for the triplet state calculated using the UHF method for selected quantum clusters. As one can clearly see in Fig. 2(a), both
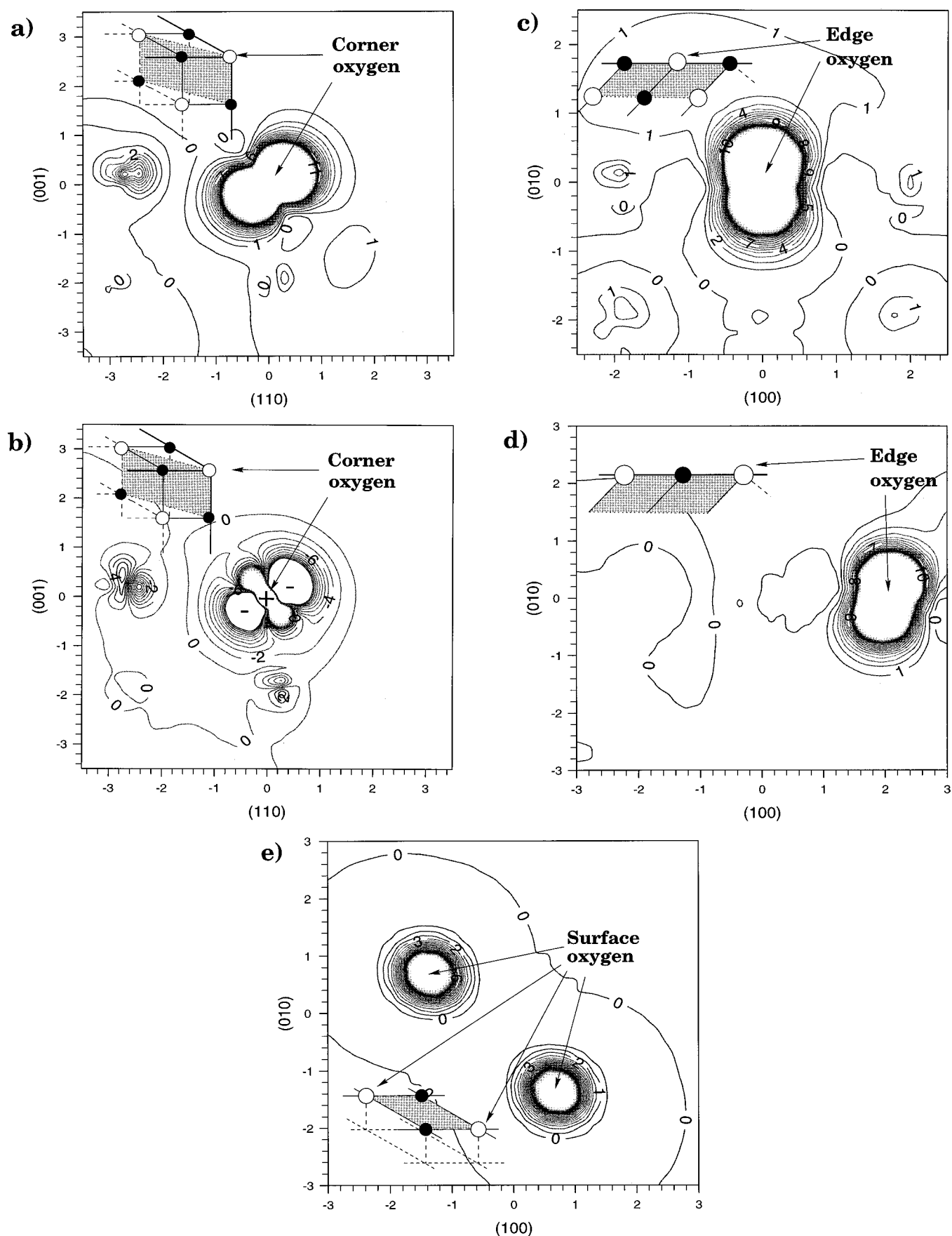
FIG. 2. Sections of the spin and differential electron density of the excited triplet state at several positions in the nanocluster. (a) The spin density at the corner site; (b) the differential electron density at the corner site; (c) the spin density at the edge calculated for the twelve ion quantum cluster [Fig. 1(f)]; (d) the spin density at the edge calculated for the four-ion quantum cluster [Fig. 1(g)]; (e) the spin density at the terrace [Fig. 1(c)].

unpaired electrons are mostly localized on the corner oxygen ion, and their density is spread out of the corner approximately along the $\langle 111 \rangle$ crystalline axis. To see how the electron excitation affects the overall electron-density distribution, in Fig. 2(b) we have plotted the section of the differential density map in the same projection as the spin density in Fig. 2(a). The difference in Fig. 2(b) is taken between the electron densities for the vertically excited triplet state calculated using CIS and the ground state. One can see that the electron-density redistribution due to the electron excitation is also mostly localized at the corner oxygen ion: there is an electron flow from a p orbital oriented along the $\langle 111 \rangle$ axis to an electronic state oriented perpendicular to that axis. The section of the spin-density plot shown in Fig. 2(c) is calculated for the 12-ion quantum cluster embedded at the edge. Again both unpaired electrons are mostly localized on only one oxygen ion, which has the lowest coordination. To check how this result can be affected by the number of quantum oxygens at the edge, in Fig. 2(d) we plotted the spin density for the linear quantum cluster Mg_2O_2 along the edge. In this case, there are two almost equivalent low-coordinated oxygen ions, one of them being closer to the nanocluster corner [see Fig. 1(g)]. Accordingly there are two almost degenerate transitions and the spin-density map is shown for one of them. The fact that the two excited states are almost degenerate indicates that for a longer edge the excited state is probably delocalized over several oxygen ions. This can be clearly seen in the case of the grain [Fig. 2(e)] the two oxygen ions in the quantum cluster are equivalent and the excited state is delocalized over both of them. Again the density of the unpaired electrons in the excited state extends perpendicular to the grain surface plane into the vacuum.

The relative total energies of the excited states at different low-coordinated surface sites could be used as the first indicator of whether the exciton excited, for instance, in the bulk or at the surface would transfer to the less coordinated edge and/or corner. In order to be able to compare the results for different shapes and sizes of quantum clusters, the relative energies of the excited states for different coordinations were estimated in the following way. First, the ionization energies $\mathbf{I}$ for the clusters included in this study were calculated using CISD. There is not much difference between the results obtained using different quantum clusters for the same location.
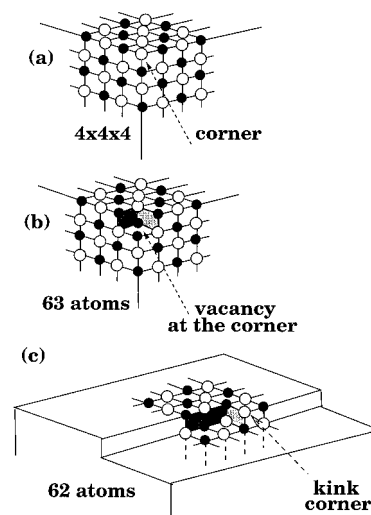
FIG. 4. Schematic of quantum clusters embedded into a $8 \times 8 \times 8$ 512-ion nanocluster used in the semiempirical Hartree-Fock calculations. To save space, only nontrivial cases are shown. The calculations for the terrace and edge were made for the same quantum cluster as shown in (a) located in the middle of the terrace and edge, respectively. Color coding is the same as in Fig. 1 and is inverted for the anion and cation corners and kinks.

In particular, the first ionization potential for the eight ion cluster at the edge [Fig. 1(f)] was found to be 8.059 eV, whereas for the 12-ion cluster shown in Fig. 1(e) we obtained 8.073 eV. However, we must admit that these ionization energies are overestimated by about 1.0–1.5 eV because the electron polarization of the nanoclusters was not accounted for in the ionized state.

Assuming the common vacuum level for all systems considered, we then placed their ground-state total energies at $-\mathbf{I}$, as shown in Fig. 3. Then the energies of the excited states were located with respect to the defined positions of the ground states using the excitation energies. As one can see in Fig. 3, the excited state in the bulk has much higher energy than that at the surface, and the latter is higher than at the edge. The energies of the excited states at the edge and at the corner appear to be very similar. Again, the absolute energies of these states are too low due to lack of polarization contribution in our calculations of the ionized and excited cluster states. Cox and Williams[5] argued that the excitation state at the surface is in the positive spectrum, our estimates suggest that it could rather have a small negative energy. Clearly this question requires more thorough investigation.

B. Semiempirical calculations for nanoclusters

The semiempirical technique allows us to use much larger quantum clusters and to perform the geometry optimization in the excited states taking into account the polarization of the rest of the nanocluster. We use these advantages in order to extend our study to more complex surface sites and to calculate the luminescence energies. This should provide a more complete comparison with experiment.

The calculations were performed for two basic nanoclusters of different sizes: $(MgO)_{108}$ and $(MgO)_{256}$ cubes. The
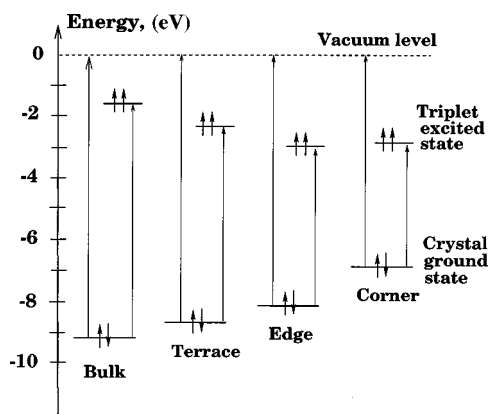

FIG. 3. Diagram representing the relative energies of the ground and excited triplet states at different positions in the nanocluster calculated using the CISD method.

TABLE II. The lowest excitation energies for the low-coordinated surface sites and the luminescence energies of relaxed excitons calculated using the embedded cluster INDO CIS method (eV).

Lowest oxygen coordination	Position	Cluster (Fig. 4)	Optical absorption edge	Luminescence	
				Singlet	Triplet[a]
5	Terrace (Ref. 16)	a	6.4[b]		5.7[b]
5	O-corner vacancy	b	4.5	4.2	3.6
4	Edge	a	5.4	4.3	3.7
4	Mg-kink	c	5.6	4.5	3.9
4	Mg-corner	a	5.3	3.5	2.9
3	O-kink	c	5.5	4.2	3.6
3	O-corner	a	4.9	3.1	2.5
3	Mg-corner vacancy	b	5.2	3.5	2.9

[a]These are estimates calculated by subtracting an average singlet-triplet splitting obtained in the Hartree-Fock calculations (see Table I), 0.6 eV, from the singlet luminescence energies (see text for discussion).
[b]These energies are given for completeness. They were calculated in Ref. 16 using a cluster embedded into the infinite (001) MgO surface and the same INDO method as used in this study with the basis set extended by floating functions.

results for these two systems are quite close and therefore we will discuss the data obtained for the larger nanocluster. The systems considered are shown in Fig. 4. In all cases we used the same cubic $(MgO)_{32}$ quantum cluster, which was embedded into the nanoclusters as shown in Fig. 4. In the kink and corner cases, both the oxygen and magnesium terminations were considered, which correspond to inverse color coding in Fig. 4. The singlet-singlet excitation and luminescence energies are summarized in Table II. They follow the same general trend as observed in the *ab initio* calculations. However, the picture is richer due to a wider variety of structures considered.

Analyzing the electron distribution in unrelaxed and relaxed excited states one can clearly distinguish two cases already noted in the *ab initio* calculations of excitation: (i) the excitation at a terminating site, such as a corner or kink; and (ii) the excitation of an ''extended'' feature, such as a monatomic step or cluster edge and terrace.

In the first case, the excited states are localized around the ion with the lowest coordination. However, the degree of localization is different. In the case of the cube corner [Fig. 4(a)], the three nearest-neighbor ions of the corner ion are equivalent and both the unrelaxed and relaxed excited states are distributed over these three neighbors. The difference in the excitation and luminescence energies for the oxygen and magnesium corners is due to the different oxygen coordinations: it is lower for the oxygen corner. In the case of the oxygen kink [Fig. 4(c)], the three nearest-neighbor cations are not equivalent and the excited state is found to be localized mostly on the Mg-O pair with the least-coordinated oxygen and magnesium ions. For the magnesium kink, the excited state is again localized on a similar pair of ions [see Fig. 4(c)], but the excitation and luminescence energies are higher because the oxygen ion is now four coordinated. The absence of the corner magnesium ion exposes three surrounding oxygens. The negative effective charge of the vacancy leads to delocalization of the excited electron over a larger number of surrounding cations.

The excited state at the cube edge was found to be more delocalized. Although it was possible to find a solution that is localized mostly on a pair of the four-coordinated oxygen and magnesium ions, the electronic state, that is delocalized over the four edge ions has an almost equivalent energy. This is similar to the result obtained in the cluster *ab initio* calculations. As will be demonstrated in the next section, the periodic calculations also demonstrate comparable features.

C. DFT calculations for periodic structures

The results of the embedded cluster calculations for the nanoclusters demonstrate that the excited states are well localized at the terminating sites such as corners and kinks, and suggest that excitation of the extended surface features, such as edges and terraces can lead to more delocalized states even after relaxation. Neither cluster nor periodic calculations can prove these conclusions due to the relatively small sizes of quantum clusters and periodic unit cells. However, the important advantage of periodic band-structure calcula-
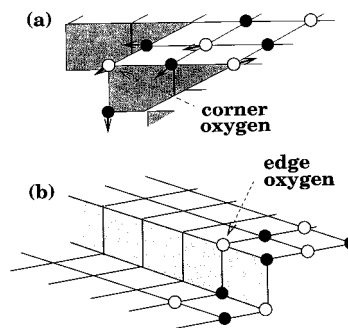

FIG. 5. Repeating geometries of the monolayer zigzag step (a) and the step (b) calculated using the DFT method. Only the topmost layer of the slab is shown explicitly. The atoms included in the primitive cell are shown by open (oxygen) and black (magnesium) circles.

TABLE III. The lowest excitation energies for the zigzag step and the monatomic step and the luminescence energies for relaxed excitons calculated within the DFT method using the CETEP and VASP codes (eV).

Oxygen coordination	Position (Fig. 5)	Number of ions in UC	Singlet-triplet excitation		Triplet-singlet luminescence	
			CETEP	VASP	CETEP	VASP
4	Monatomic step	44	3.73	4.56	3.43	4.20
		66	3.63	5.61	3.3	5.5
3	Zigzag step	44	3.21	4.08	1.75	3.04

tions is that they allow us to test these conclusions further due to the much stronger interaction between the localized and delocalized crystal states. For this purpose, we turn to two characteristic cases: a monatomic zigzag step and a monatomic step shown in Figs. 5(a) and 5(b). The corner sites of the zigzag step are oxygen-terminated [Fig. 5(a)]. Geometrically, the zigzag steps are only slightly different from the kinks treated in the previous section: the oxygen ion at the zigzag step corner has two equivalent nearest neighbor magnesium ions, i.e., this is a more symmetric structure than the oxygen kink [Fig. 4(c)]. The monatomic step edge [Fig. 5(b)] represents a more extended surface feature than the steps and edges of the finite nanoclusters (Figs. 1 and 4). Therefore, if the relaxed excited state will prove to be localized, this will provide more strong evidence in favor of exciton localization at low-coordinated surface sites.

The geometric structures of both step systems in the ground (singlet) state were optimized in Ref. 39 using the CETEP code. Essentially the same slab models were used in the present calculations. For the zigzag step system we used a repeating supercell consisting of 44 atoms [Fig. 5(a)], while for the standard step system two repeating supercells consisting of two and three primitive cells along the step [see Fig. 5(b)] and 44 and 66 ions were employed.

The excitation and luminescence energies between the lowest singlet (ground) and triplet (excited) states calculated using the CETEP and VASP codes are presented in Table III. First of all, we notice that there is a substantial difference (up to 2.2 eV) between the energies obtained by the two methods. To check the dependence of the results on the number of $\mathbf{k}$ points, we repeated the ground and excited states calculations for the zigzag-step system using five $\mathbf{k}$ points instead of two with both codes. The obtained geometries of the relaxed ground and excited states were almost identical to those calculated using two $\mathbf{k}$ points, and both the excitation and luminescence energies changed by less than 0.05 eV. Since the same DFT functional is used in both cases and the $\mathbf{k}$-point sampling used in the calculations was found to be sufficient, we suggest that the discrepancy between the two methods comes from different pseudopotentials. However, at this stage it is difficult to prove whether this is the only cause and a more detailed study is certainly needed to understand the accuracy of both DFT methods with respect to singlet-triplet transition energies.

As one can see in Table III, both methods nevertheless give the same trend and similar relative energies in regard to the dependence of transition energies on coordination: the lower the oxygen coordination, the smaller transition energies. This is consistent with the result obtained above with

other methods. It is worth also mentioning that the relaxed geometries of the ground and excited states obtained using the two methods agree with each other to within 2–3 % of the anion-cation distance $a_0 = 2.122$ Å used in all calculations.

Let us now turn to a more detailed analysis of the results for the zigzag step. The nature of the excited state after the vertical transition can be understood better after studying the differential electron density plotted in Fig. 6(a). This is the difference between the electron densities of the excited and ground states at the same geometry. One can see that, as in the cluster calculations for the cube corner [Fig. 2(b)], the electron redistribution due to the electron excitation is mostly confined to the oxygen states demonstrating strong oxygen polarization. The geometric structure of this excited state was then optimized with respect to the positions of ions in the repeating cell. The strongest displacements (about $0.08a_0$) were found for the magnesium ions nearest to the corner oxygen. Their directions are shown by arrows in Fig. 5(a). The corner oxygen is displaced slightly outwards the corner, and the nearest oxygen ion is shifted in the direction of the corner oxygen by about $0.07a_0$. This relaxation is characteristic of a hole localized on the corner oxygen. This is indeed confirmed by the spin-density plot presented in Fig. 6(b). It is very similar to that shown in Fig. 2(a) and demonstrates that the two unpaired electrons in the relaxed triplet state are mainly localized on the oxygen ions. A significant portion of the spin density, which is not seen in the figure, is localized in the ''pockets'' of the zigzag-step structure [Fig. 5(a)]. The spin density is the largest on the corner oxygen and decays rapidly inside the lattice. This suggests the exciton localization around the corner oxygen, which is qualitatively similar to the results obtained for the cube corners above.

The transition energies calculated for the step shown in Table III are generally larger than for the corner system. The dependence on the number of ions in the unit cell is more pronounced in the VASP calculations. However, independent of the size of the supercell, the displacements of the ions in this excited state are much smaller than those obtained for the zigzag step and do not exceed $0.03a_0$. The discrepancies between the ionic displacements calculated using the VASP and the CETEP codes are of the same order as the displacements themselves.

In all cases, we find that the spin density is strongly localized around the step edge. However, the details of localization along the step were dependent on the size of the unit cell. In the 44-atom cell, there are only two independent oxygen atoms at the step edge and the spin density appears to
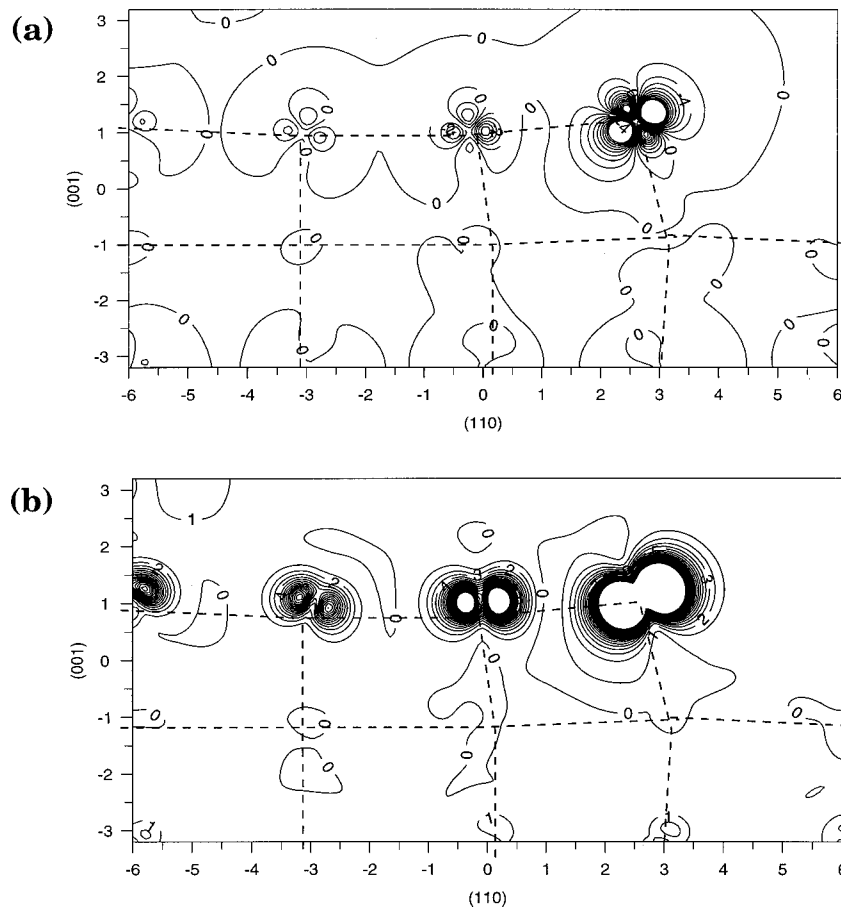
FIG. 6. Sections of the differential and spin electron densities of the zigzag step: (a) the differential electron density of the unrelaxed excited triplet state; (b) the spin density of the fully relaxed excited triplet state. The section is made as in Figs. 2(a), and 2(b) through the corner oxygen ion along the $\langle 110 \rangle$ axis perpendicular to the terrace plane. The atomic network indicated by dashed lines reflects the atomic relaxation. Other notations are the same as in Fig. 2. Note the polarization and decay of the differential and spin-electron density inside the lattice.

be localized equally on both of them [Fig. 7(a)]. There is also significant concentration of the spin density outside the step opposite to the step-edge Mg atoms. In the 66-atom step system there are already three independent oxygens at the step edge. In this case, using CETEP we obtained only one stable triplet configuration in which the spin density was localized on the two nearest edge oxygens with the Mg edge atom in between [Fig. 7(b)]. (Note also significant spin density opposite to this Mg atom outside the step edge.) Using VASP we found a similar solution, but with slightly more diffuse spin-density distribution. However, there is also another solution with 0.2 eV lower energy, which corresponds to the state that is completely delocalized over three oxygens at the edge. Existence of several almost degenerate solutions is consistent with the relatively small atomic displacements in the triplet state and with very small (about 0.01 eV) deviations of the total energies per atom for all systems studied.

Thus, we conclude that the results obtained with the DFT method are qualitatively consistent with those obtained with other methods: (i) the transition energies tend to decrease with the reduced coordination of the surface oxygen atom; and (ii) the fully relaxed triplet exciton is localized at the

three-coordinated oxygen corner on the zigzag step. It is also localized at the step but is likely to be extended along it.

IV. DISCUSSION

The results of calculations of the excitation and luminescence energies for the low-coordinated sites in nanoclusters and at surfaces of MgO using different techniques demonstrate qualitatively very similar features. For the excitation energies, the most reliable data are obtained using the embedded cluster *ab initio* Hartree-Fock calculations that we discuss first.

First, independent on the basis set used, the results show a very consistent dependence of the excitation energies on the oxygen coordination, $n = 3, \ldots, 6$. The differences between the excitation energies for $\Delta n = 1$ are of the order of 1 eV, which is close to the experimental results.[3] If we assume that the singlet-triplet splitting is not very much affected by the electron correlation, we can estimate the energies of the correlated singlet-singlet transitions too. For this purpose, we use the splitting values obtained in the CIS calculations and the singlet-triplet transition energies obtained using CISD (see Table I). The excitation energies estimated in this way
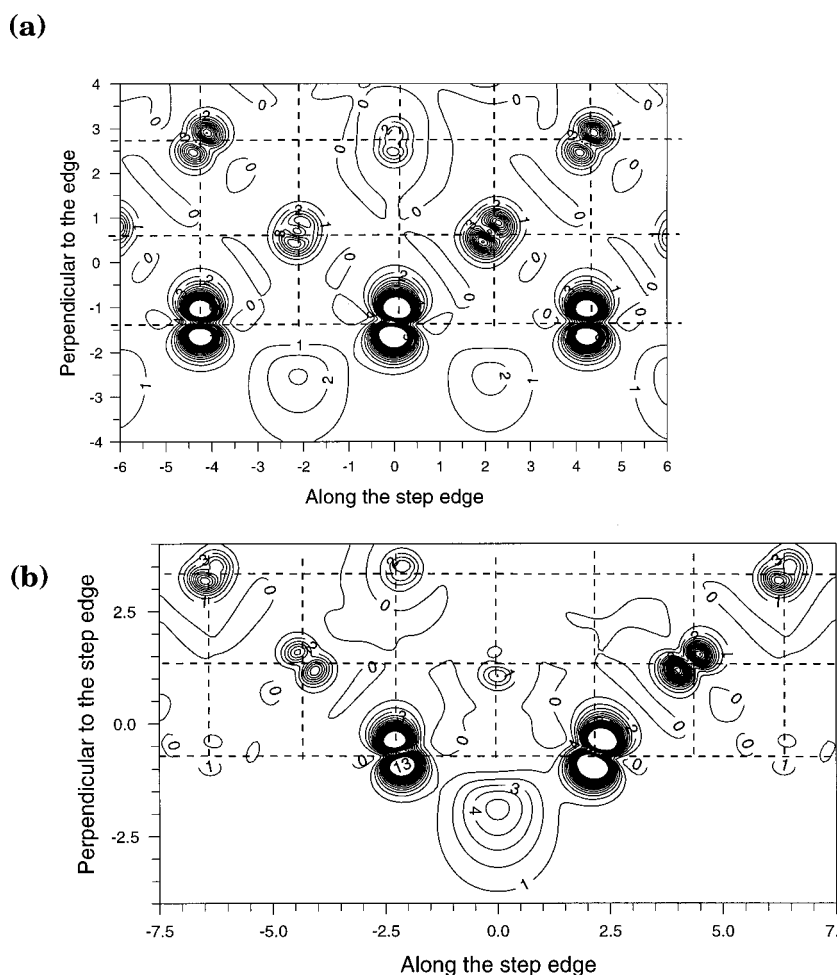
(a)

(b)

FIG. 7. Sections of the spin-electron density of the fully relaxed excited triplet state at the monatomic step calculated using the CETEP code: (a) for the 44-atom periodic system; and (b) for the 66-atom periodic system. Dashed lines indicate the atomic network of the upper terrace of the step and reflect the atomic relaxation. The section is made along the terrace with the normal of the section plane perpendicular to the surface. Other notations are the same as in Figs. 2 and 6.

are presented in the last column of Table I. The CISD energies are in good agreement with the experimental data for the bulk[4] and the surface.[5] Direct comparison with the results of Garrone, Zecchina, and Stone[3] on the ultraviolet diffuse reflectance spectra of microcrystallites is impossible because the experimental spectra are averaged over many different low-coordinated sites. Nevertheless, our results qualitatively support the assignment of the peaks at about 5.7 and 4.6 eV to the four- and three-coordinated oxygen surface sites respectively.[3]

Second, both the spin-density distribution in the excited state and the differential electron density between the ground and excited states demonstrate the strong contribution of the oxygen states into the excited state. This is not something one would expect based on a traditional view that the bottom of the conduction band in ionic insulators is mainly determined by cation states. We note that the calculations by Pandey, Zuo, and Kunz[14] suggest complete exciton localization on the oxygen ion in the bulk of MgO: Cluster calculations by Bagus, Illas, and Sousa[15] demonstrate an opposite behavior of the excited electron: it is completely delocalized over the entire cluster. However, the latter result could be related to the fact that the quantum cluster in Ref. 15 was surrounded by a point ion array.

Third, the excited states appear to be more localized at the terminating three-coordinated oxygen sites, than within the edge or at the surface. The similar trend is also obtained in our DFT calculations for the monatomic zigzag step and the monatomic step. The relative energies of the excited states corresponding to oxygen sites of different coordination suggest the possibility of the excitation transfer from, for example, the surface to the more localized terminating corner sites with lower energy. Similar behavior of the excitation was proposed in Ref. 7 on the basis of analysis of the experimental data, however, the mechanism of this process requires more detailed study.

The results obtained using the parameter-free methods allow us to verify our semiempirical calculations. The parameters of these calculations were optimized to reproduce the band-gap excitation in the bulk MgO (7.8 eV) using a periodic model and the CIS method. With this calibration, the agreement with the results of the *ab initio* CIS calculations for the excitation energies at the low-coordinated sites is quite satisfactory.

Spectroscopic features similar to those discussed above have also been observed in the excitation spectra of the photoluminescence of powdered MgO.[7–10] In particular, all of them have a narrow peak with the maximum at about 4.6 eV

and strong absorption with the maximum at energies greater than 5.5 eV. However, the experimental photoluminescence spectra[7–10] are inhomogeneous and much broader than the excitation spectra, with a maximum around 3.3 eV and a long tail up to 2.0 eV, which could be decomposed into several lines. This implies a variety of photoluminescence centers. Our semiempirical and DFT calculations of the luminescence energies suggest that the lowest energies correspond to the terminating sites. They do not give a final answer as to whether the excited states can localize at the step or at the grain edge and whether these surface features can serve as the luminescence centers. However, taken together with the calculated relative energies of excited states (Fig. 3), they are consistent with the evidence[7,8] that the excitation can be transferred from the surface to the terminating sites where the luminescence takes place.

The results of semiempirical and parameter-free calculations demonstrate that the excited states at the corner sites are strongly localized around the low-coordinated oxygen ion. The unrelaxed and relaxed triplet states have lower energies than the corresponding singlet states. These results suggest that the experimentally estimated long (more than several microseconds) lifetimes of photoluminescence could be due to the triplet-singlet transitions within the strongly localized terminating sites.

The luminescence energies calculated by the semiempirical technique are for the singlet-singlet transitions. Due to the small relaxation of the excited state we can assume that the singlet-triplet splittings between the relaxed singlet- and triplet-excited states could be of the same order as those calculated for the excitation energies using the Hartree-Fock method and CIS, i.e., about 0.6 eV. Subtracting this value from the calculated energies of the singlet-singlet transitions we can estimate the triplet-singlet luminescence energies. These are presented in the last column of Table II. One can see that the luminescence energies calculated using the INDO method and the CIS technique are generally higher than the spectral region of ∼2.0–3.7 eV, which accommodates the photoluminescence spectra. This could be because of the rather uncontrollable way the electron correlation is included in the INDO parameters. As one can see in Table I, the calculations using CISD systematically shift the excitation energies down by about 1.1–1.4 eV with respect to CIS results. We hoped that more accurate luminescence energies could be obtained using the DFT calculations. However, the discrepancy of the results obtained with two codes does not allow us to reach quantitative conclusions. Finally, we note that the luminescence energies obtained for the kink sites are higher than these for the corners and the corner vacancies. This is in agreement with the experimental observation that the excitation of powders with the 4.52 eV photons eliminates luminescence with energies higher than 3.5 eV. In terms of our model this would mean preferential excitation at the corner sites which excludes energy transfer to the step kinks.

These results lend strong support to the model of photoluminescence of powdered MgO proposed by Coluccia and co-workers,[7–10] which suggests that the luminescence centers correspond to the low-coordinated surface sites. They demonstrate dependence of the luminescence energies on particular surface sites and general reduction of the luminescence energies with reduced coordination of ions.

The strong dependence of the excitation and luminescence energies on ion coordination obtained in this paper is due to the combination of several interrelated factors. Some of them have already been discussed by Garrone, Zecchina, and Stone[3] and include the reduction of the Madelung potential at low-coordinated sites, which leads to their substantial relaxation with respect to ideal geometry and to strong electron-density redistribution. As was pointed out by Garrone, Zecchina, and Stone,[3] the reduction of the Madelung potential alone cannot quantitatively explain the experimental data without considering the two other factors, and even in this case the agreement with experiment is not perfect. This is perhaps not surprising because, as is demonstrated in our calculations, both the degree of localization of the excited state and its nature depend on its location. Strong localization of the excited states on the oxygen ions makes the Madelung argument even less applicable.

One may then ask how do these results depend on nanocluster size and on whether this is a finite cluster or an infinite surface. Qualitatively this can be illustrated by comparing the densities of states for the monatomic step and the zigzag step. The excited state is more localized at the zigzag step and the corresponding occupied and vacant states are better separated from the band states than in the case of monatomic step. Similar observation applies to the cluster calculations: the occupied and vacant states associated with the electron and hole of the exciton at the corner are much better separated from the other states than at the edge or terrace. Providing the excited states are well localized, as at corners or kinks, the spin-density distribution [see Figs. 2(a) and 6(a)] and the electronic states are very similar in the cluster and periodic calculations. However, if the extent of localization of the excited state starts to exceed the size of a quantum cluster or a periodic cell both character of localization and comparison between finite clusters and infinite periodic structures become less reliable.

To summarize, the results of our study emphasize the feasibility of several effects that can be important in spectroscopic studies of real surfaces, and could be used in studies of molecular adsorption at surface sites, photocatalytic surface processes, and DIET. These are: (i) the strong dependence of spectroscopic properties on coordination and the possibility of selective optical excitation of low-coordinated surface sites; (ii) the energy transfer from the sites with higher coordination to those with lower coordination and finally to the localization centers.

[1] J. D. Levine and P. Mark, Phys. Rev. **144**, 751 (1966).

[2] E. V. Stefanovich and T. N. Truong, J. Chem. Phys. **102**, 5071 (1995).

[3] E. Garrone, A. Zecchina, and F. S. Stone, Philos. Mag. B **42**, 683 (1980).

[4] D. M. Roessler and W. C. Walker, Phys. Rev. **159**, 733 (1959).

[5] P. A. Cox and A. A. Williams, Surf. Sci. **175**, L782 (1986).

[6] A. Zecchina, M. G. Lofthouse, and F. S. Stone, J. Chem. Soc., Faraday Trans. 1 **71**, 1476 (1975).

[7] S. Coluccia, A. M. Deane, and A. Tench, J. Chem. Soc., Faraday Trans. 1 **74**, 2913 (1978).

[8] S. Coluccia, A. J. Tench, and R. L. Segall, J. Chem. Soc., Faraday Trans. 1 **75**, 1769 (1979).

[9] S. Coluccia, A. Barton, and A. J. Tench, J. Chem. Soc., Faraday Trans. 1 **77**, 2203 (1981).

[10] S. Coluccia and L. Marchese, in *International Symp. on Acid-Base Catalysis*, edited by K. Tanabe, H. Hattori, T. Yamaguchi, and T. Tanaka (Kodansha, Tokyo, 1988).

[11] W. W. Duley, Philos. Mag. B **49**, 159 (1984).

[12] K. S. Song and R. T. Williams, *Self-Trapped Excitons* (Springer-Verlag, Berlin, 1993).

[13] P. W. Fowler and P. Tole, Surf. Sci. **197**, 457 (1988).

[14] R. Pandey, J. Zuo, and A. B. Kunz, Phys. Rev. B **39**, 12 565 (1989).

[15] P. S. Bagus, F. Illas, and C. Sousa, J. Chem. Phys. **100**, 2943 (1994).

[16] A. L. Shluger, C. R. A. Catlow, R. W. Grimes, and N. Itoh, J. Phys.: Condens. Matter **3**, 8027 (1991).

[17] J. S. J. Hargreaves, G. J. Hutchings, R. W. Joyner, and C. J. Kiely, J. Catal. **135**, 576 (1992).

[18] P. J. Ziemann and A. W. Castleman, Jr, J. Chem. Phys. **94**, 718 (1991).

[19] E. Knozinger, K.-H. Jacob, S. Singh, and P. Hofmann, Surf. Sci. **290**, 388 (1993).

[20] J. D. Gale, J. Chem. Soc., Faraday Trans. **93**, 69 (1997).

[21] M. J. Frisch, G. W. Trucks, H. B. Schlegel, P. M. W. Gill, B. G. Johnson, M. A. Robb, J. R. Cheeseman, T. A. Keith, G. A. Petersson, J. A. Montgomery, K. Raghavachari, M. A. Al-Laham, V. G. Zakrzewski, J. V. Ortiz, J. B. Foresman, J. Cioslowski, B. B. Stefanov, A. Nanayakkara, M. Challacombe, C. Y. Peng, P. Y. Ayala, W. Chen, M. W. Wong, J. L. Andres, E. S. Replogle, R. Gomperts, R. L. Martin, D. J. Fox, J. S. Binkley, D. J. Defrees, J. Baker, J. P. Stewart, M. Head-Gordon, C. Gonzalez, and J. A. Pople, GAUSSIAN94 (edition E.1) (Gaussian, Inc., Pittsburgh, PA, 1995).

[22] A. L. Shluger and J. D. Gale, Phys. Rev. B **54**, 962 (1996).

[23] A. L. Shluger, L. N. Kantorovich, A. I. Livsits, and M. J. Gillan, Phys. Rev. B **56**, 15 332 (1997).

[24] A. L. Shluger, A. L. Rohl, D. H. Gay, and R. T. Williams, J. Phys.: Condens. Matter **6**, 1825 (1994).

[25] A. L. Shluger, A. L. Rohl, and D. H. Gay, Phys. Rev. B **51**, 13 631 (1995).

[26] W. R. Wadt and P. J. Hay, J. Chem. Phys. **82**, 284 (1985).

[27] J. B. Foresman and A. Frisch, *Exploring Chemistry with Electronic Structure Methods* (Gaussian, Inc., Pittsburgh, PA, 1996).

[28] K. Hermann and P. S. Bagus, Phys. Rev. B **17**, 4082 (1978).

[29] J. Q. Broughton and P. S. Bagus, Phys. Rev. B **36**, 2813 (1987).

[30] A. E. Reed, R. B. Weinstock, and F. Weinhold, J. Chem. Phys. **83**, 735 (1985).

[31] J. B. Foresman, M. Head-Gordon, and J. A. Pople, J. Phys. Chem. **96**, 135 (1992).

[32] J. A. Pople, R. Seeger, and R. Krishnan, Int. J. Quantum Chem., Symp. **11**, 149 (1977).

[33] J. A. Pople and D. L. Beveridge, *Approximate Molecular Orbital Theory* (McGraw-Hill, New York, 1970).

[34] E. V. Stefanovich, E. K. Shidlovskaya, A. L. Shluger, and M. A. Zakharov, Phys. Status Solidi B **160**, 529 (1990).

[35] B. G. Dick and A. W. Overhauser, Phys. Rev. **112**, 90 (1958).

[36] R. Car and M. Parrinello, Phys. Rev. Lett. **55**, 2471 (1985).

[37] L. J. Clarke, I. Stich, and M. C. Payne, Comput. Phys. Commun. **72**, 14 (1992).

[38] L. Kleinman and D. M. Bylander, Phys. Rev. Lett. **48**, 566 (1980).

[39] L. N. Kantorovich, J. M. Holender, and M. J. Gillan, Surf. Sci. **343**, 221 (1995).

[40] L. N. Kantorovich and M. J. Gillan, Surf. Sci. **374**, 373 (1997).

[41] M. C. Payne, M. P. Teter, D. C. Allan, T. A. Arias, and J. D. Joannopoulos, Rev. Mod. Phys. **64**, 1045 (1992).

[42] G. Kresse and J. Furthmuller, Phys. Rev. B **54**, 11 169 (1996).

[43] G. Kresse and J. Furthmuller, Comput. Mater. Sci. **6**, 15 (1996).

[44] D. Vanderbilt, Phys. Rev. B **41**, 7892 (1990).

[45] K. Laasonen, A. Pasquarello, R. Car, C. Lee, and D. Vanderbilt, Phys. Rev. B **47**, 10 142 (1993).

[46] J. P. Perdew, in *Electronic Structure in Solids' 91*, edited by P. Ziesche and H. Eschrig (Academie Verlag, Berlin, 1991).

[47] J. P. Perdew, J. A. Chevary, S. H. Vosko, K. A. Jackson, M. R. Pederson, D. J. Singh, and C. Fiolhais, Phys. Rev. B **46**, 6671 (1992).

[48] O. Gunnarsson and B. I. Lundqvist, Phys. Rev. B **13**, 4274 (1976).

[49] T. Ikeda, N. B. Wong, D. O. Harris, and R. W. Field, J. Mol. Spectrosc. **68**, 452 (1977).

[50] A. L. Shluger, J. D. Gale, and C. R. A. Catlow, J. Phys. Chem. **96**, 10 389 (1992).

[51] W. C. Mackrodt, J. Chem. Soc., Faraday Trans. 2 **85**, 541 (1989).

[52] S. Veliah, R. Pandey, Y. S. Li, J. M. Newsam, and B. Vessal, Chem. Phys. Lett. **235**, 53 (1995).